2007. 2
Master's Thesis

A study on the Mechanical characteristics for fillet Joints of Al 5083 alloy by using Hybrid welding

Graduate School of Chosun University

Department of Naval Architecture and Ocean Engineering

HO – KYOUNG PARK

A study on the Mechanical characteristics for fillet Joints of Al 5083 alloy by using Hybrid welding

하이브리드 용접에 의한 Al 5083 합금의
필렛용접부 용접특성 연구

February 2007

Graduate School of Chosun University

Department of Naval Architecture and Ocean Engineering

HO – KYOUNG PARK

A study on the Mechanical characteristics for fillet Joints of Al 5083 alloy by using Hybrid welding

Advisor : Professor Han-Sur Bang

A Thesis submitted for the degree of

Master of Engineering

October 2006

Graduate School of Chosun University

Department of Naval Architecture and

Ocean Engineering

HO – KYOUNG PARK

朴 鎬 慶의 碩士學位 論文을 認准함

委員長　朝鮮大學校 敎授　房 熙 善 _____

委　員　朝鮮大學校 敎授　房 漢 瑞 _____

委　員　朝鮮大學校 敎授　尹 德 榮 _____

2006 年　11 月

朝鮮大學校大學院

CONTENTS

List of Figure.....3

List of Table.....4

ABSTRACT.....5

Chapter 1 Introduction.....6

1. 1 Background and Purpose.....6

1. 2 Basic theory.....6

Chapter 2 Hybrid & MIG Weldability of Al 5083 alloy.....15

2. 1 Experimental set-up.....15

2. 2 Characteristics of Object Materials.....15

2. 3 Principle of Hybrid Welding Process.....17

2. 3. 1 MIG welding process.....17
2. 3. 2 Hybrid welding process.....18

2. 4 Experiment of Fillet Joint Welding by Hybrid Welding Process.....19

2. 4. 1 Effect of MIG welding & Hybrid welding process.....19
2. 4. 2 Effect of Hybrid(Laser + MIG)welding combine angle & focusing position.....20
2. 4. 3 Effect of gap bridging ability.....21

2. 5 Result & Discussion of experiment.....22
(Weld beads appearance, geometry & dimension by transverse cross-sections)

2. 5. 1 MIG welding & Hybrid welding process.....22
2. 5. 2 Hybrid(Laser + MIG)welding combine angle & focusing position.....24
2. 5. 3 Gap bridging ability.....26

Chapter 3 Numerical Simulation of Hybrid Welds.....28

3. 1 Thermal distribution of Hybrid welding.....31
3. 2 Thermal history of Hybrid welding.....32
3. 3 Welding residual stress distribution in weldment.....32
3. 4 Heat input details.....34

Chapter 4 Mechanical strength Test.....35

4. 1 Hardness test in welds.....35

Chapter 5 Conclusion.....36

References.....38

Acknowledgements.....40

List of Figure

Figure. 1. 1 Structure of the Heat transfer analysis program…….7
Figure. 1. 2 Structure of the Residual stress analysis program……. 9
Figure. 2. 1 Principle of experimental set-up focal angle of incident for Laser & Arc……...10
Figure. 2. 2 Schematic of MIG welding process…….12
Figure. 2. 3 Schematic of Hybrid welding process……. 13
Figure. 2. 4 Principle of experimental set-up for welding process……. 14
Figure. 2. 5 Principle of experimental set-up for welding process……. 15
Figure. 2. 6 Principle of experimental set-up for welding process……. 16
Figure. 2. 7 Bead shapes of fillet joints by each welding process……...18
Figure. 2. 8 Leg Length & Throat Size of Specimens…….18
Figure. 2. 9 Cross section of MIG/ Laser/ Hybrid (Laser+Arc, Arc+Laser) fillet joints…….19
Figure. 2. 10 Bead shapes & Cross-section of fillet joints by Hybrid welding
Combine & focusing position……20
Figure. 2. 11The relation between bead profile, bead width in the upper part
and the lower part welding speed for bead on plate welding by hybrid welding……21
Figure. 2. 12 Bead shapes&Cross-section of fillet joints by Hybrid welding gap bridging ability….22
Figure. 3. 1 Physical properties of Al 5083 and Al 5356 for heat conduction analysis……...23
Figure. 3. 2 Mechanical properties for thermal elasto-plastic analysis……... 24
Figure. 3. 3 Strain-hardening parameter for thermal elasto-plastic analysis (Al 5083) ……. 24
Figure. 3. 4 Mesh division of weldments……..25
Figure. 3. 5 Boundary Condition for thermal elasto-plastic analysis……..25
Figure. 3. 6 Thermal distribution of the Laser-Arc welding, Arc-Laser welding……26
Figure. 3. 7 Thermal history in Laser-Arc welding, Arc-Laser welding……..27
Figure. 3. 8 Residual stress distribution in Laser-Arc welding, Arc-Laser welding……28
Figure. 3. 9 Schematic diagram of the optimization welding condition……. 29
Figure. 3. 10 Penetration depth variations based on the focal position gap width
and angle between the welding axis and flange plate……29
Figure. 4. 1 Hardness value in Hybrid Welds(Laser+MIG) ……30

List of Table

Table. 2. 1 Chemical composition of A5083 for base material……11
Table. 2. 2 Chemical composition of A5356 for wire……..11
Table. 2. 3 Range of welding parameters…….15
Table. 2. 4 Range of welding parameters…….16
Table. 2. 5 Range of welding parameters…….17

ABSTRACT

하이브리드 용접에 의한 Al 5083 합금의 필렛용접부 용접특성 연구

Ho-Kyoung Park
Advisor : Professor Han-Sur Bang, Ph.D.
Department of Naval Architecture and
Ocean Engineering
Graduate School of Chosun University

최근 수송수단의 경량화를 통한 연료비 절감 및 자원재생을 목적으로 고강도 알루미늄 합금의 사용이 증가하고 있는 추세이다. 그러나 수송기계(선박)용 5XXX 계열 고강도 알루미늄 합금은 일반 철에 비해 융점이 낮을 뿐만 아니라 큰 열 팽창과 높은 반사율로 인해 현장적용에 어려움이 많다.

따라서 본 논문은 알루미늄 5083 합금에 대한 필렛용접기법을 적용하기 위해 3KW 연속파 Nd:YAG 레이저와 MIG 용접기법을 복합한 하이브리드 필렛용접의 현장적용 가능성에 대해 기술하였다.

현장 적용 가능성을 검토하기 위하여 본 논문은 용접 시 용접공정변수(선행 프로세스, Laser+MIG 토치의 각도, 레이저 조사위치, 갭의 영향)최적화와 용접부 역학적 거동을 이해하기 위해 각 용접에 대한 시험편을 제작하여 실험을 실시 하였으며 유한요소법에 의한 열전도 해석과 열탄소성 해석을 실시하여 각 용접부의 역학적 거동, 즉 용접 열 분포 및 용접 잔류응력을 비교 분석 하였다.

본 연구를 토대로 최적의 용접조건을 선정할 수 있었으며 기존의 용접법과 비교해 약 2 배의 용접속도 향상과 건전한 용접부를 얻을 수 있었다. 또한 하이브리드 필렛용접부의 용융부 및 열 열향부의 경계와 일치함을 확인 할 수 있었으며 하이브리드 필렛용접에 있어서 선행 용접공정에 의한 용접부 형상과 잔류응력의 분포가 변화함을 확인 할 수 있었다. 또한 기계적 실험(경도시험)을 통하여 강도측면에서 기존 용접법에 비해 하이브리드 용접법이 장점을 가짐을 확인하였다.

Chapter 1 Introduction

1. 1 Background and Purpose

Since the weight reduction of vehicles is strongly required, the production of high-strength aluminum alloy is continuing to increase. In particular, the aluminum- magnesium (Al-Mg) alloy sheets are widely used in car industries and ship building, replacing steel sheets and fibre reinforced plastic panels, due to their excellent properties such as high strength, corrosion resistance and general good weldability.

In spite of its excellent properties, the difficulties to weld aluminum are due to their characteristics of material. For example, the main characteristics of aluminum alloy influencing weldability are low melting point, high thermal and electrical conductivity, large thermal expansion and contraction ratio, and surface oxidation, etc. In this study, the laser-arc hybrid welding was applied to develop and apply alternative fusion welding process for aluminum alloy.

For this purpose, the characteristics of process parameters (laser & arc combine angle, laser-arc distance (LAD) and focal position of hybrid head to specimen) are investigated for hybrid fillet joint. Relation between process parameter and profile of cross section area has been investigated with the characteristics of optical aspects of weldment formed by hybrid welding (HAZ and weld metal microstructures). Reliability assessment and verification of the welding design and construction criteria for welds formed by hybrid welding are conducted through the experiment.

1. 2 Basic theory

1. 2. 1 The basic consideration of welding heat distribution in weldment.

The heat supplied by a welding arc produces complex thermal cycles and flows from the hotter parts to the cooler. This phenomenon is expressed by "Fourie's law" (2. 1), the rate of flow of heat, per unit time per unit area, in the direction of x direction. That is

$$\rho c \frac{\partial T}{\partial t} = \lambda \nabla^2 T + \dot{Q} \tag{1.1}$$

where T is temperature (℃), ρ is density (g/㎤), $\dot{Q}$ is rate of temperature change due to heat generation per volume (cal/㎤・sec), t is time (sec), λ is thermal conductivity of isotropic material

(cal/cm · sec · ℃) and c is specific heat (cal/g · ℃).

To solve this equation of un-stationary heat conduction, following boundary conditions are applied according to the kinds of problem.

• When the temperature is determined on the boundary S_1:

$$T = \overline{T} \tag{1.2}$$

where $\overline{T}$ is determined temperature.

• When the heat flux, q_0, flows from the boundary S_2:

$$q = q_0 \tag{1.3}$$

• When heat transfer is on the boundary S_3 for convection:

$$q = \alpha_c (T - T_c) \tag{1.4}$$

where α_c is heat transfer coefficient for convection (cal/cm^2 · sec · ℃), T is boundary temperature of the object (℃), and T_c is the outside temperature of the object (℃).

• When heat radiation is on the boundary S_4:

$$q = \sigma F (T^4 - T_r{}^4) \tag{1.5}$$

where σ is the Stefan Boltzmann constant, F is a compensation coefficient of shape, and T_r is the temperature of radiation source (℃). This equation can be transformed to the form of linear equation for the ease of processing as follows:

$$q = \alpha_r (T - T_r) \tag{1.6}$$

where

$$\alpha_r = \sigma F (T + T_r)(T^2 + T_r{}^2) \tag{1.7}$$

Heat flux, q (cal/cm^3 · sec · ℃), in normal direction on the boundary is derived from the Fourier law as below:

$$q = -\lambda \frac{\partial T}{\partial n} \tag{1.8}$$

Heat conduction problem for the object of analysis is formulated as the finite element method using Galerkin method. Internal temperature of the element, T, is given by

$$T(x, y, z, t) = [N(x, y, z)]\{\phi(t)\} \tag{1.9}$$

where $[N]$ is a shape function matrix shown the relation between nodal temperature and internal temperature of the element. $\{\phi\}$ is the vector of the nodal temperature of the element at time t.
If Galerkin method is applied in equation (1.1) using $[N]$ as a weighting function at this time, following equation is obtained.

$$\int_{V^e} [N]^T \left\{ \lambda \left(\frac{\partial^2 T}{\partial x^2} + \frac{\partial^2 T}{\partial y^2} + \frac{\partial^2 T}{\partial z^2} \right) + \dot{Q} - \rho c \frac{\partial T}{\partial t} \right\} dV = 0 \tag{1.10}$$

where superscript, T, shows transformation of matrix and subscript, V^e, shows the domain of element. The term of second order in partial differential equation (1.10) is changed using Green-Gauss theorem, a formula of partial integration, to the following equation.

$$\begin{aligned} &\int_{V^e} \lambda [N]^T \left(\frac{\partial^2 T}{\partial x^2} + \frac{\partial^2 T}{\partial y^2} + \frac{\partial^2 T}{\partial z^2} \right) dV = \\ &- \int_{V^e} \lambda \left(\frac{\partial [N]^T}{\partial x} \frac{\partial T}{\partial x} + \frac{\partial [N]^T}{\partial y} \frac{\partial T}{\partial y} + \frac{\partial [N]^T}{\partial z} \frac{\partial T}{\partial z} \right) dV + \int_{S^e} \lambda [N]^T \left(\frac{\partial T}{\partial n} \right) dS \end{aligned} \tag{1.11}$$

where S^e is the boundary of element.
If equation (1.9) and equation (1.2), Fourier's law, are substituted in equation (1.11), the right side of equation (1.11) becomes as bellows:

$$- \int_{V^e} \lambda \left(\frac{\partial [N]^T}{\partial x} \frac{\partial [N]}{\partial x} + \frac{\partial [N]^T}{\partial y} \frac{\partial [N]}{\partial y} + \frac{\partial [N]^T}{\partial z} \frac{\partial [N]}{\partial z} \right) dV \cdot \{\phi(t)\}$$

$$-\int_{S^e} q[N]^T dS \tag{1.12}$$

Using equation (1.12), equation (1.10) becomes finally as follows:

$$-\int_{V^e} \lambda\left(\frac{\partial[N]^T}{\partial x}\frac{\partial[N]}{\partial x}+\frac{\partial[N]^T}{\partial y}\frac{\partial[N]}{\partial y}+\frac{\partial[N]^T}{\partial z}\frac{\partial[N]}{\partial z}\right)dV\cdot\{\phi(t)\}$$

$$-\int_{S^e} q[N]^T dS+\int_{V^e}\dot{Q}[N]^T dV-\int_{V^e}\rho c[N]^T[N]dV\cdot\frac{\partial\{\phi(t)\}}{\partial t}=0 \tag{1.13}$$

Simplifying above equation (1.13), un-stationary heat conduction problem can be expressed as following finite element expression for an element.

$$[k]\{\phi\}+[c]\left\{\frac{\partial\phi}{\partial t}\right\}=\{f\} \tag{1.14}$$

where $[k]$, $[c]$ and $\{f\}$ show the heat conductivity matrix of an element, the heat capacity matrix of an element and the heat flow vector of an element, respectively. They are expressed as follows:

$$[k]=\int_{V^e}\lambda\left(\frac{\partial[N]^T}{\partial x}\frac{\partial[N]}{\partial x}+\frac{\partial[N]^T}{\partial y}\frac{\partial[N]}{\partial y}+\frac{\partial[N]^T}{\partial z}\frac{\partial[N]}{\partial z}\right)dV \tag{1.15}$$

$$[c]=\int_{V^e}\rho c[N]^T[N]dV \tag{1.16}$$

$$\{f\}=\int_{V^e}\dot{Q}[N]^T dV-\int_{S^e} q[N]^T dS \tag{1.17}$$

Boundary conditions on the boundary S_2 to S_4 can be given to substitute q in second term of equation (1.17) using equation (1.3), (1.4) and (1.6).

• When the heat flux, q_0, flows from the boundary S_2:

From the equation (1.3), $$\int_{S_2^e} q[N]^T dS=\int_{S_2^e} q_0[N]^T dS \tag{1.18}$$

In the case of adiabatic boundary condition, q_0 become zero (0).

• When heat transfer is on the boundary S_3 for convection:

From the equation (1.4), $$\int_{S_3^e} q[N]^T dS = \int_{S_3^e} \alpha_c (T - T_c)[N]^T dS \quad (1.19)$$

If T in the equation (1.19) is substituted by the equation (1.9), the equation (1.19) become as bellows:

$$\int_{S_3^e} q[N]^T dS = \int_{S_3^e} \alpha_c [N]^T [N] dS \cdot \{\phi(t)\} - \int_{S_3^e} \alpha_c T_c [N]^T dS \quad (1.20)$$

• When heat radiation is on the boundary S_4:

From the equation (1.6), $$\int_{S_4^e} q[N]^T dS = \int_{S_4^e} \alpha_r (T - T_r)[N]^T dS \quad (1.21)$$

If T in the equation (1.21) is substituted by the equation (1.9), The equation (1.21) becomes as bellows:

$$\int_{S_4^e} q[N]^T dS = \int_{S_4^e} \alpha_r [N]^T [N] dS \cdot \{\phi(t)\} - \int_{S_4^e} \alpha_r T_t [N]^T dS \quad (1.22)$$

From the above conditions, general boundary condition eliminated first boundary condition when the temperature is determined on the boundary S_1 can be applied to solve the un-stationary heat conduction problem.

Equation (1.15) and (1.17) are modified using equation (1.18), (1.20) and (1.22) as follows:

$$[k] = \int_{V^e} \lambda \left(\frac{\partial [N]^T}{\partial x} \frac{\partial [N]}{\partial x} + \frac{\partial [N]^T}{\partial y} \frac{\partial [N]}{\partial y} + \frac{\partial [N]^T}{\partial z} \frac{\partial [N]}{\partial z} \right) dV + \int_{S_3^e} \alpha_c [N]^T [N] dS + \int_{S_4^e} \alpha_r [N]^T [N] dS \tag{1.23}$$

$$\{f\} = \int_{V^e} \dot{Q} [N]^T dV - \int_{S_2^e} q_0 [N]^T dS + \int_{S_3^e} \alpha_c T_c [N]^T dS + \int_{S_4^e} \alpha_r T_r [N]^T dS \tag{1.24}$$

Therefore, finite element formula of an element can be derived as a form of matrix equation including boundary conditions by using equation (1.16), (1.23) and (1.24).

Finite element formula for the whole object analysed is constructed with assembled each matrix of elements and it can be expressed as follows:

$$[K]\{\Phi\} + [C]\left\{\frac{\partial \Phi}{\partial t}\right\} = \{F\} \tag{1.25}$$

where $[\Phi]$, $[K]$, $[C]$ and $\{F\}$ show the vector of the nadal temperature in the whole object, the heat conductivity matrix in the whole object, the heat capacity matrix in the whole object and the heat flow vector in the whole object, respectively. They are given as bellows.

$$[\Phi] = \sum_e \phi, \ [K] = \sum_e k, \ [C] = \sum_e c, \ \{F\} = \sum_e f \tag{1.26}$$

In this study, the heat conduction analysis is carried out using the two dimensional heat conduction programs by equation.

1. 2. 1. 1 Heat transfer analysis program

Using this formulation the finite element code is developed for the heat transfer analysis.
The developed code consist of 28 subroutines and according to the task performed, subroutines can be grouped accordingly as shown in the block diagram of Fig. 1. 1.

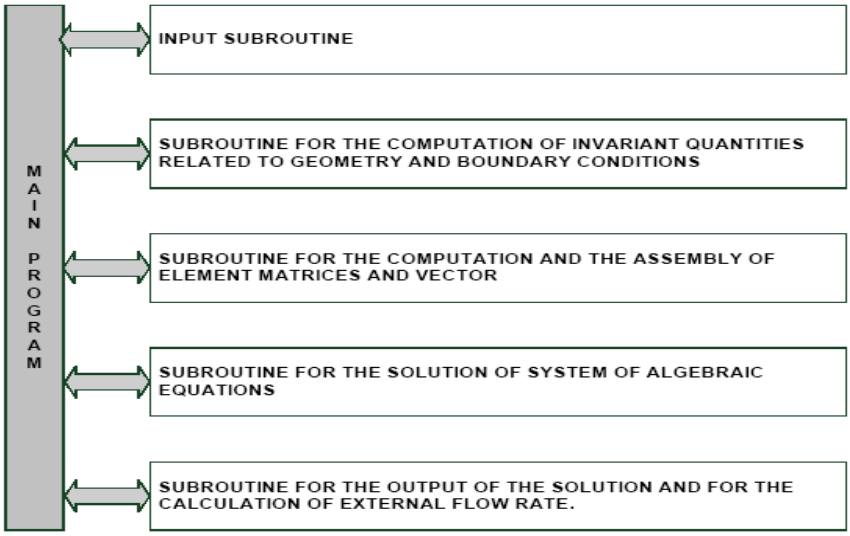

Figure. 1. 1 Structure of the Heat transfer analysis program

1. 2. 2 The basic consideration of elastic-plastic analysis in weldment.

The solid is assumed to be Iso-tropic media for welding residual stress analysis and the mechanical properties of material (yield stress, Young's modulus, thermal expansion coefficient) are dependent of temperature change in both elastic and plastic region.
In the plastic region, the Plastic-flow theory is adopted, besides, Von-Mises condition is used as the yield function considering linear equivalent hardening law. The relations used in this analysis are as follows.

1. 2. 2. 1 Total strain relation

$$\varepsilon_T = \varepsilon^e + \varepsilon^p + \varepsilon^t \qquad (1.\ 27)$$

where, ε^e : elastic strain , ε^p : plastic strain , ε^t : thermal strain

1. 2. 2. 2 Nodal force-Nodal displacement relation

According to the Principal of virtual work, the equivalent nodal force increment of element { dF } is as follow.

$$\{dF\} = [K]\{dU\} - \{dL\} \tag{1. 28}$$

where, $[K] = \int_v [B]^T [D][B] dv$: stiffness matrix of element,

$\{dL\} = \int_v [B]^T [C] dT dv$: equivalent nodal force by heat.

1. 2. 2. 3 Stress-Strain relation

If the increment of stress is $[C]dT$, considering the temperature dependence of physical properties, the stress-strain relation is written as equation(1. 28)

$$\{d\sigma\} = [D]\{d\varepsilon\} - [C]dT \tag{1. 29}$$

where, $[D^e]$: elastic stress-strain matrix,

ε^t : thermal strain

a : coefficient of linear expansion.

1. 2. 2. 4 Stress-Strain relation in elastic region

If the material behave in elastic region, the total strain is the summation of thermal strain and elastic strain and expressed as follows.

$$\{C\}:[D]^e \alpha \frac{1}{E} - \frac{E - E_1}{\Delta T}\{\sigma\}$$

where, E_1 : Young's modulus after temperature change (ΔT)

1. 2. 2. 5 Stress-Strain relation in plastic region

Total strain increment $\{d\varepsilon\}$ is the summation of elastic, plastic and thermal strain, the total strain equation can be written as follow

$$\{d\varepsilon\} = \{d\varepsilon^e\} + \{d\varepsilon^p\} + \{d\varepsilon^t\} \tag{1. 30}$$

$$\{d\sigma\} = [D^e\{d\varepsilon\} - [D^e]\{\frac{\partial f}{\partial \sigma}\}\lambda - [D^e]\{\alpha\}T + \frac{d[D^e]}{dT}[D^e]^{-1}\{\sigma\}dT$$

1. 2. 2. 6 Residual stress analysis program

The developed code consist of 47 subroutines and according to the task performed, subroutines can be grouped accordingly as shown in the block diagram of Fig. 1. 2.

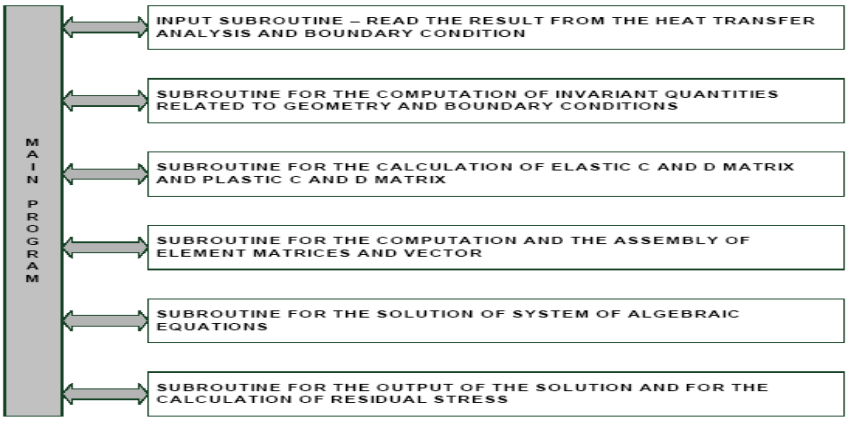

Figure. 1. 2 Structure of the Residual stress analysis program

Chapter 2 Hybrid & MIG weldability of Al 5083 alloy

2. 1 Experimental Set-up

For the experiment, 3 kw CW Nd:YAG laser was used together with conventional welding equipment consisting of a welding mode DAIHEN 500A A6442. The MIG torch was connected close to the laser focusing optic at an angle of about 55°. Shielding gas was supplied through a MIG torch located at the side of laser head. Laser beam was irradiated perpendicularly to the surface of specimen. Experimental setup for CW Nd:YAG laser, MIG and hybrid welding is shown in Fig. 2. 1

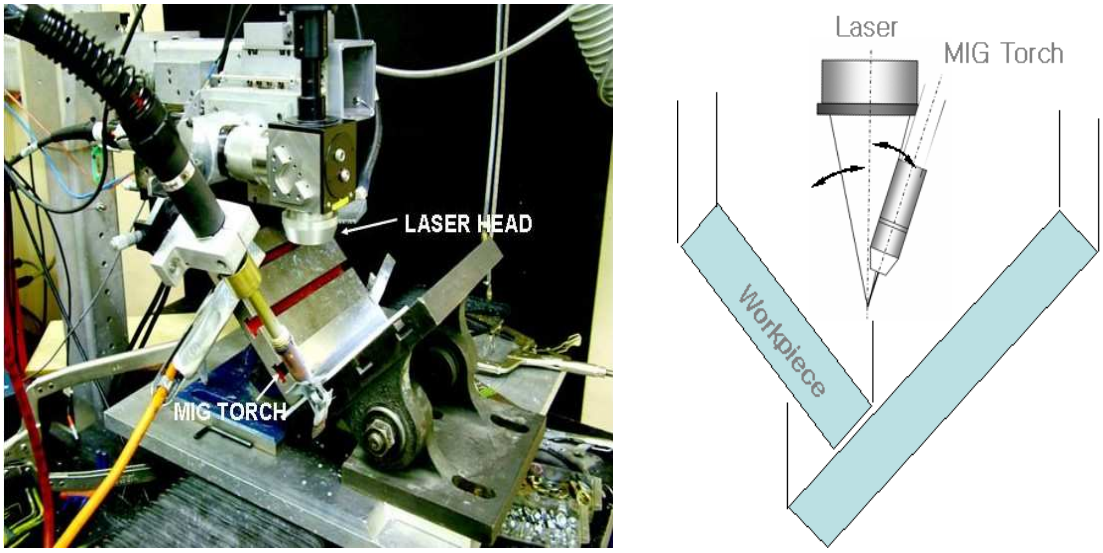

Figure. 2.1 Principle of experimental set-up focal angle of incident for Laser & Arc

2. 2 Characteristics of Object Materials

Marine grade A5083 series alloys, non heat treatable aluminum alloys, are selected in this study for their high strength to weighting ratio combined excellent corrosion resistance and general good weldability, in marine environment. They have large quantities of magnesium in solid solution for their strengthening. A5083 is the established industry standard. Chemical composition of A5083 has been given in Table. 2. 1.

Table. 2. 1 Chemical composition of A5083 for base material

Si	Fe	Cu	Mn	Mg	Cr	Zn	Ti	Other elements		Aluminium
								Each	Total	
0.40	0.40	0.10	0.40 ~ 1.0	4.0 ~ 4.9	0.05 ~ 0.25	0.25	0.15	0.05	0.15	Rem.

In general, the filler alloy selected should be similar in composition to the base metal. Resistance to hot cracking and porosity is an important standard of judgment for weldability in non-heat treatable aluminum alloys. In the case of hot cracking, high constrained conditions and/or high susceptibility to cracking are main cause. Especially, hot cracking may be occurred in weld metal when welding is conducted for 5XXX series alloy that have low range magnesium content (0.5 to 2.5 wt% Mg). To avoid cracking, use of a high-magnesium filler alloy is recommended. A5356 filler alloy is recommended to A5083 base metal alloy by industrial standard. Chemical composition of A5356 filler alloy has been given in Table. 2. 2

Table. 2. 2 Chemical composition of A5356 for wire

Si	Fe	Cu	Be	Mn	Mg	Cr	Zn	Ti	Other elements		Aluminium
									Each	Total	
0.25	0.40	0.10	0.0008	0.05 ~ 0.20	4.5 ~ 5.5	0.05 ~ 0.20	0.10	0.06 ~ 0.20	0.05	0.15	Rem.

Oxide film on the surface is very adherent and if removed reforms rapidly. This is a cause of oxide related defects such as lack of fusion and oxide entrapment; therefore, this has to be removed properly by mechanical and/or chemical methods. The melting point (about 2060℃) of aluminum oxide (Al_2O_3) is much higher than that (about 660℃) of the pure aluminum. The oxide melts and forms s slag that floats on the top of weld pool. Proper inert gas shielding is needed to prevent reformation of oxide film during welding.

2. 3 Principle of Hybrid Welding

2. 3. 1 MIG welding Process

MIG (metal inert gas) welding process (Fig. 2. 2) is an arc welding process that joins metals together by heating them with an electrode arc that is established between consumable electrode and work pieces.

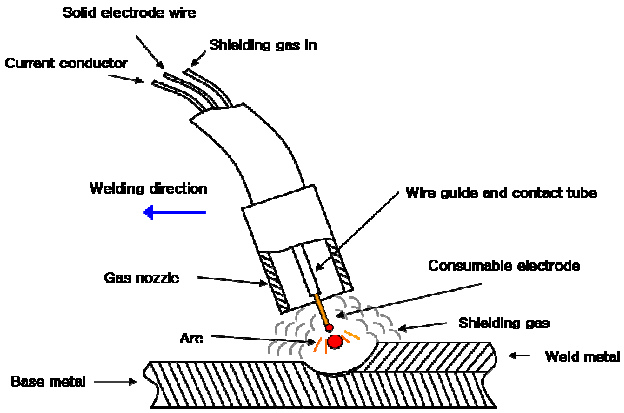

Figure. 2. 2 Schematic of MIG welding process

From the MIG welding process, the total transfer of heat ($H.I$) to the weldment per unit time and unit length is given by:

$$H.I = \eta_A \frac{EI}{V}$$

where E is voltage, I is current, V is welding speed, and η_A is the heat transfer efficiency

The important variables of MIG welding process to affect weld penetration, bead geometry and weld quality are as follows:

- Welding current (electrode wire feed speed)
- Arc voltage (arc length)
- Electrode extension
- Electrode diameter
- Polarity
- Welding speed
- Electrode orientation (welding gun angle)

In general, arc current can be changed with the slight changes in the arc voltage (arc length) and wire feeding speed. The vast majority of MIG welding process utilizes DCEP (direct current electrode positive) condition because it provides a stable arc, low spatter, a good weld bead profile and the greatest depth of penetration.

2. 3. 2 Hybrid welding Process

Laser (light amplification by stimulated emission of radiation) welding process is a high energy density welding process that joins metals together by heating them with a collimated and coherent radiation. The laser radiation leads to a very narrow heat affected zone (HAZ) with a large ratio of welding depth to seam width (deep weld effect) and low distortion due to low specific energy input. It can reach very high welding speed. However, the gap bridging ability of the laser welding process is very low due to its small focus diameter (about 0.3~0.6 mm)

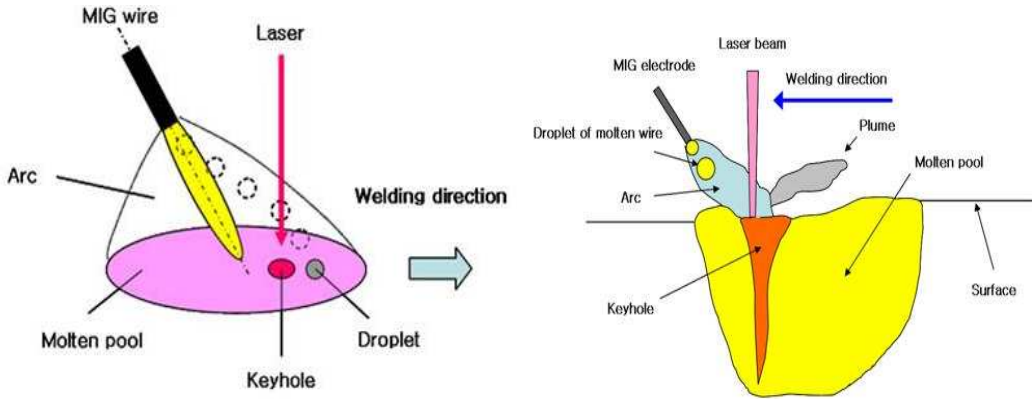

Figure. 2. 3 Schematic of Hybrid welding process

The absorptivity of aluminum at room temperature is reported around 2 % where a CO_2 laser (10.6 ㎛) is used, but 5~10 % when a Nd:YAG laser (1.06 ㎛) is used. This means that Nd:YAG laser system may be suitable for the joining of aluminum.

In the laser system, electrical operating efficiency (or wall-plug efficiency) is very low and its value is only of the order of between 5 and 10% in CO_2 laser system and of the order of between 1 and 3 % in Nd:YAG laser system. Its capital investment in equipment is still expensive.

In the case of Nd:YAG laser welding, argon (Ar) with high atomic weight (39.948) is used. The high atomic weight of Ar atoms helps to sweep the vapour particles out of the pass of the incident laser beam. The heavy argon atoms are also useful to blanket the molten pool and shield it against oxidation. Also, loss of beam power can be occurred in the reflective and transmissive optics.

From the laser welding process, the total transfer of heat ($H.I$) to the weldment per unit time and unit length can be given simply as follows:

$$H.I = \eta_L \frac{P}{V}$$

where P_W is beam power of laser at workpiece, V is welding speed, and η_L is the heat transfer efficiency.

The important independent process variables of laser welding process to affect depth of penetration and metallurgical and mechanical properties are as follows:

- Incident laser beam power
- Incident laser beam diameter
- Absorptivity
- Welding speed

Besides weld design, shielding gas, depth of focus, etc., also have important roles. The depth of penetration in laser welding process is mainly dominated by the power density (incident power per unit area) is a function of incident laser beam power and beam diameter. Laser beam diameter is also important because spatial distribution of energy is changed as laser beam diameter is changed in various beam modes.

2. 4 Experiment of Fillet Joint Welding by Hybrid Welding Process

2. 4. 1 Effect of MIG welding & Hybrid welding process

The selected material for this study is Al 5083 alloy. Experimental setup for CW Nd:YAG Laser, MIG and hybrid welding are shown Fig 2. 4. A specimen size of 100 mm wide and 250 mm long & 5 mm thickness were used. The surface of specimen was cleaned using Acetone. The employed welding conditions for CW Nd:YAG Laser, MIG and hybrid welding are shown in Table 2. 3

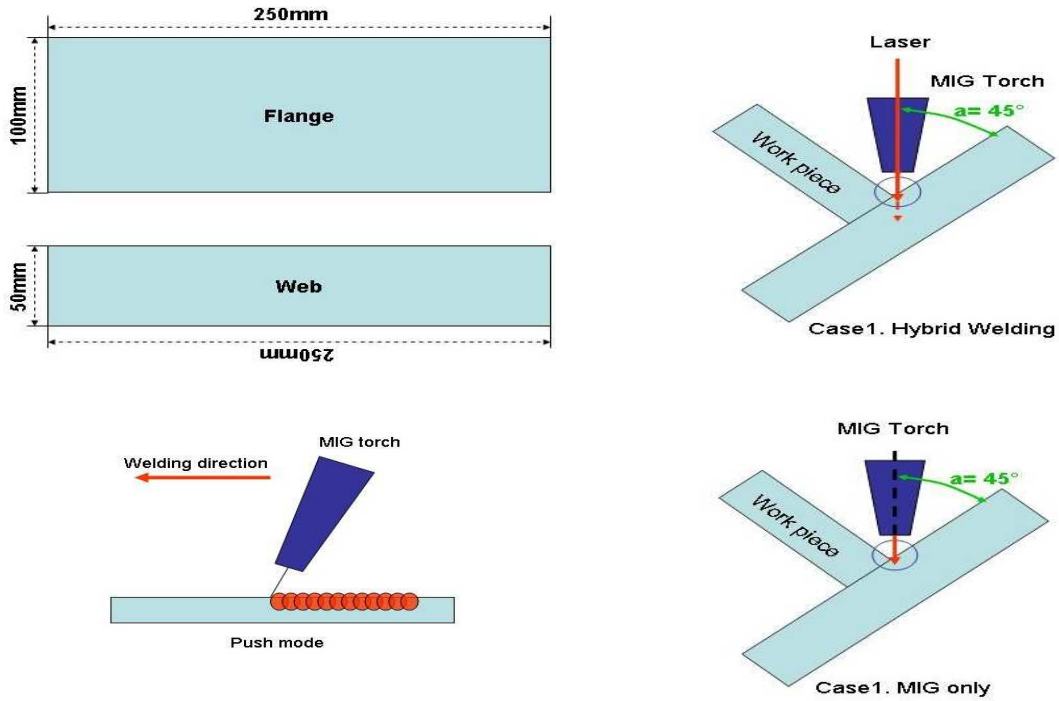

Figure. 2. 4 Principle of experimental set-up for welding process

Table. 2. 3 Range of welding parameters

Parameters / Exp. No	MIG Only			Laser Only	**Laser-Arc Hybrid**	
	200906-03	200906-04	200906-05	200906-06	**220906-01-L**	**220906-02-M**
Ave. current(A)/Ave. voltage(v)	194/23.2	194/23.2	194/23.2		**194/23.2**	**194/23.2**
WFS (m/min)	6	6	6		**6**	**6**
WELDING SPEED (m/min)	**1**	**0.7**	**0.6**		**1**	**1**
LASER POWER (kW)				**2.76**	**2.76**	**2.76**
FOCAL LENGTH (mm)				200	**200**	**200**
DEFOCUSED DEPTH (mm)				0	**0**	**0**
MIG TORCH ANGLE (°)				35	**35**	**35**
SHIELDING GAS (L/min)	**Ar 30**	**Ar 30**	**Ar 30**	**Ar 30**	**Ar 30**	**Ar 30**
LASER -ARC DISTANCE (mm)					**3**	**3**

In this study, for the initial test, the angle between Hybrid head and flange angle was kept 45 degrees and incidence position was a contact line. The gap size was approximately zero mm with considering gap tolerance.

2. 4. 2 Effect of Hybrid(Laser + MIG)welding combine angle & Focusing position

Experimental setup for hybrid welding was shown Fig 2. 5. A specimen size of 100 mm wide and 250 mm long & 5 mm thickness were used. The surface of specimen was cleaned using Acetone. The employed welding conditions for hybrid welding are shown in Table 2. 4.

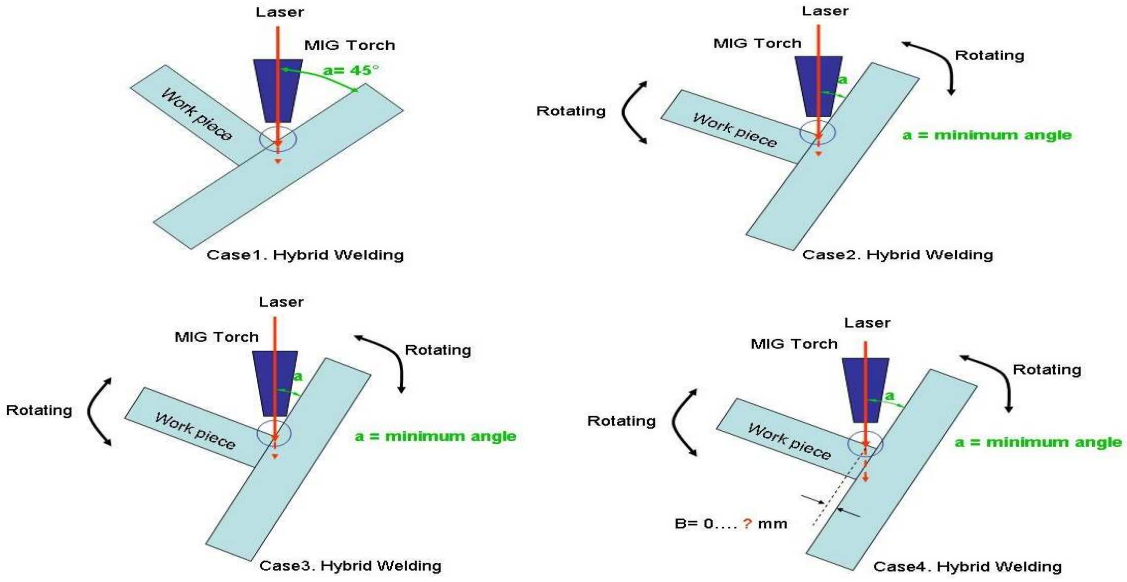

Figure. 2. 5 Principle of experimental set-up for welding process

Table. 2. 4 Range of welding parameters

Parameters / Exp. No	Laser-Arc Hybrid			
	201006-01	201006-02	201006-03	201006-04
Ave. current(A)/Ave. voltage(v)	194/23.2	194/23.2	194/23.2	194/23.2
WFS (m/min)	6	6	6	6
WELDING SPEED (m/min)	1	1	1	1
LASER POWER (kW)	**3**	**3**	**3**	**3**
Gap tolerance (mm)	**No gap**	**No gap**	**No gap**	**No gap**
FOCAL POINT(mm)	**0**	**1**	**0**	**1**
FLANGE ANGLE (°)	**45**	**45**	**55**	**55**
SHIELDING GAS (L/min)	Ar 20	Ar 20	Ar 20	Ar 20
LASER -ARC DISTANCE (mm)	3	3	3	3

In this study, for the second test, the angle between Hybrid head and flange angle was kept 45, 55, 60 degrees and the focal position 0 mm, 0.5 mm, 1mm. The gap size was approximately zero mm with considering gap tolerance.

2. 4. 3 Effect of Gap bridging ability

Experimental setup for hybrid welding are shown Fig 2. 6. A specimen size of 100 mm wide and 250 mm long & 5 mm thickness were used. The surface of specimen was cleaned using Acetone. The employed welding conditions for hybrid welding are shown in Table 2. 5.

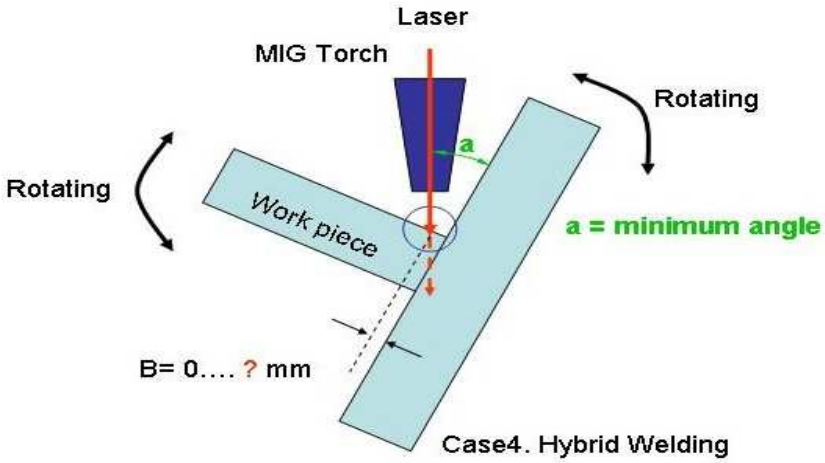

Figure. 2. 6 Principle of experimental set-up for welding process

Table. 2. 5 Range of welding parameters

Parameters / Exp. No	**Laser-Arc Hybrid**			
	301006--06	301006-07	301006-08	301006-09
Ave. current(A)/Ave. voltage(v)	194/23.2	194/23.2	194/23.2	194/23.2
WFS (m/min)	6	6	6	6
WELDING SPEED (m/min)	1	1	1	1
LASER POWER (kW)	**3**	**3**	**3**	**3**
Gap tolerance	**0**	**1**	**1.5**	**2**
FOCAL POINT(mm)	**1**	**1**	**1**	**1**
Flange ANGLE (°)	**55**	**55**	**55**	**55**
SHIELDING GAS (L/min)	Ar 20	Ar 20	Ar 20	Ar 20
LASER -ARC DISTANCE (mm)	3	3	3	3

In this study, for the final test, the angle between Hybrid head and flange angle was kept 55 degrees and the focal position 0 mm, 1mm. The gap size was approximately 0 mm, 1mm, 2mm with considering gap tolerance.

2. 5 Result & Discussion of Experiment

- Weld beads appearance, geometry & dimension by transverse cross-sections

2. 5. 1 MIG welding & Hybrid welding process

In the case of MIG welding for fillet joints, welding speed about 1000mm/min is too fast to form sufficient weld bead shape. Furthermore, web and flange were not welded completely because of incomplete fusion. However, the 600 and 700mm/min were quite good for making proper weld bead except proper throat size and leg length.

Even if laser welding has benefits for inducing good welds it is really difficult to make good joint design as aspects of structure and strengthen due to not enough throat size and leg length.

There were two cases of hybrid welding like laser leading and MIG leading conditions. Many previous research reports, generally, mentioned that laser leading process causes good welds except gap bridging condition.

As below figure (exp. No 220906-01), laser leading process has less contamination and spatter because laser induce plasma near the molten pool is effective in stabilizing the arc.

In MIG leading case, occurrence of contamination and spatter were increased as compared with laser leading condition. Moreover, it seems to be humping beads because welding speed was too fast with strong arc force and incomplete fusion.

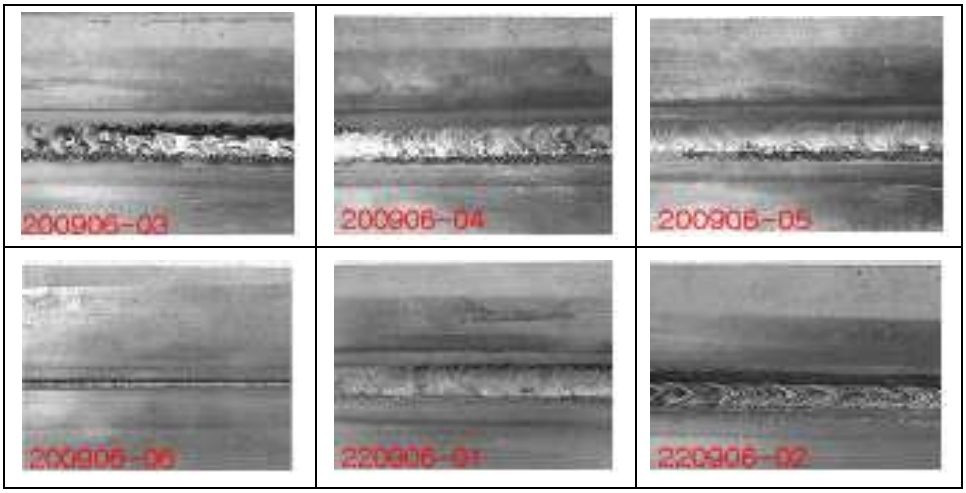

Figure 2.7 Bead shapes of fillet joints by each welding process; No.200906-03 MIG in 1000mm/min welding speed, No. 200906-04 MIG in 700mm/min welding speed, No. 200906-05 MIG in 600mm/min welding speed, No. 200906-06 Laser welding, No. 220906-01 Laser-arc hybrid welding, No. 220906-02 Arc-laser hybrid welding.

From the result of cross section, the all of specimen have not enough penetration because of MIG pulsing which occurs that the energy of heat input only used for wire melting. Therefore, those specimens are hardly welded.

For the structural strength point of view, the leg length and throat size for fillet joints are very important. However, the laser welding of fillet joints, especially, was not sufficient for leg length and throat size of fillet joints. There were almost zero throat sizes and unclear leg lengths. In the comparison between MIG processes and Hybrid welding processes, the throat size of MIG case are slightly bigger than Hybrid case due to the less surface tensile force and viscosity of melted aluminum. Even though hybrid processes have smaller throats than MIG processes there were better penetrations.

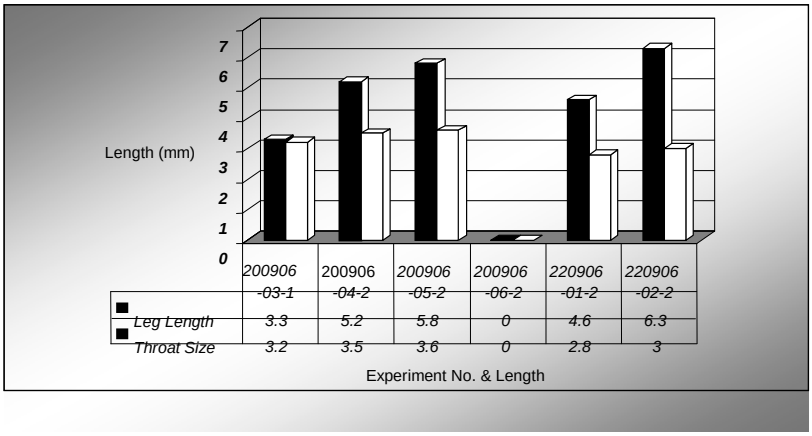

Figure 2. 8 Leg Length & Throat Size of Specimens

Note: The quality imperfection of arc T-joint is inapplicable to the welds of laser welding.

In the hybrid welding case, the interaction of laser beam and arc induced a quite good penetration for fillet joints than other cases. And also a chink between web and flange induct molten pool moving because of the less viscosity and density of the chink part. However, as below figure (exp. No 220906-02-2), MIG leading process has many pores.

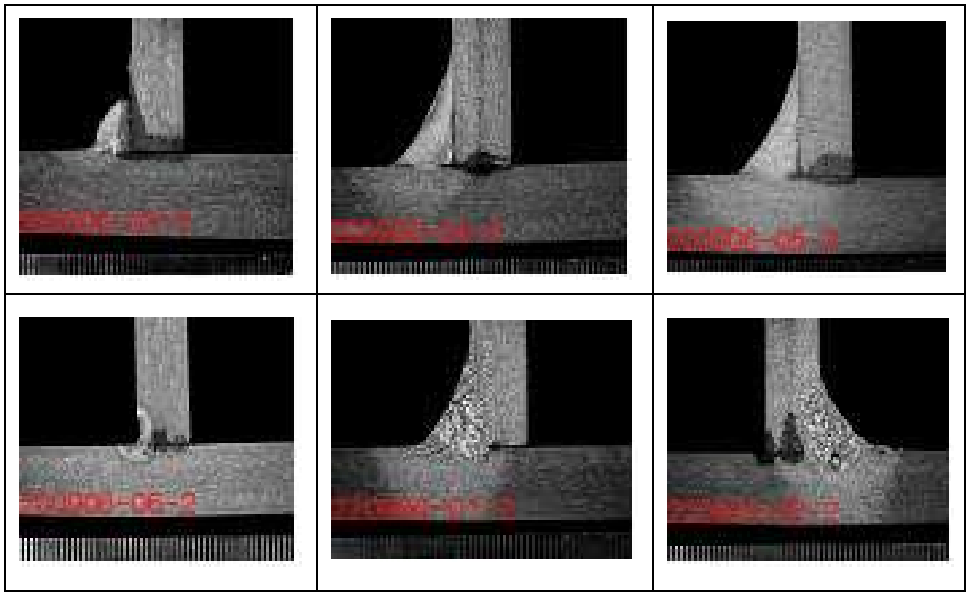

Figure 2. 9 Cross section of MIG/ Laser/ Hybrid (Laser+Arc, Arc+Laser) fillet joints; No.220906-03 MIG in 1000mm/min welding speed, No. 220906-04 MIG in 700mm/min welding speed, No. 220906-05 MIG in 600mm/min welding speed, No. 200906-06 Laser welding, No. 220906-01 Laser-arc hybrid welding, No. 220906-02 Arc-laser hybrid welding.

2. 5. 2 Hybrid(Laser + MIG) welding combine angle & focusing position

From the result of cross section about combine angle & focusing position, despite of increasing laser power(2.76kw–3kw)all of the specimen have not enough penetration. Compared with about 3kw laser power and 2.76kw laser power, welds bead shape & cross-section found not enough penetration in the case of the hybrid fillet welding. In this study, combine angle & focusing position have not an effect on the Hybrid fillet welding to gain full penetration.

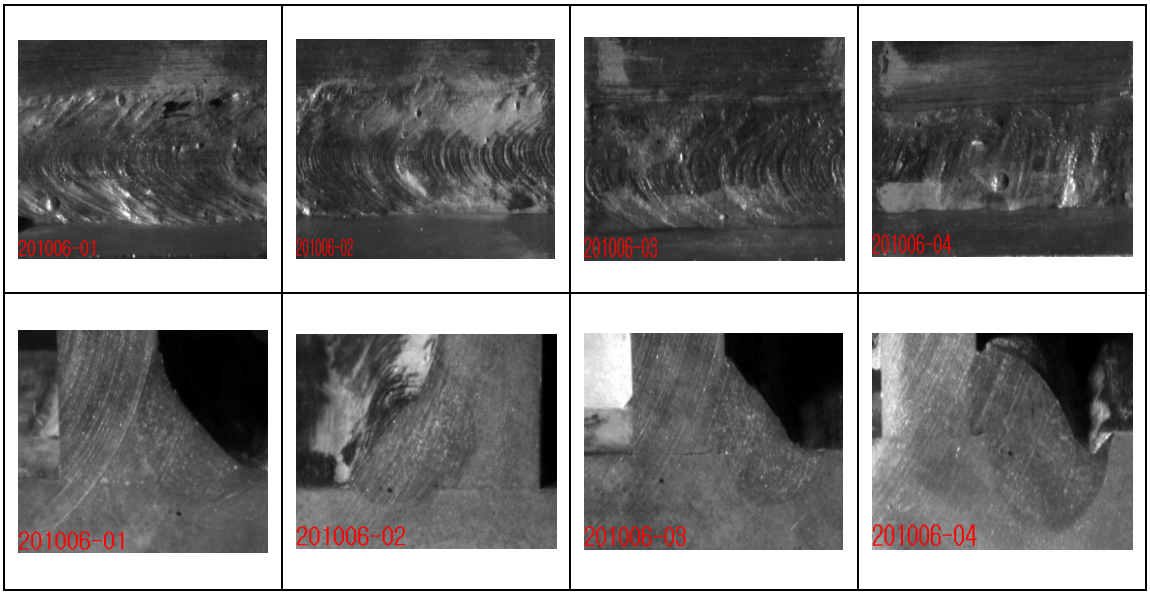

Figure 2.10 Bead shapes&Cross-section of fillet joints by Hybrid welding combine&focusing position(Laser power:3KW/194A/23.2V/Welding speed:1m/min/No gap/Ar:20L/min/WFS:6m/min) No.201006-01:angle-45°/ position-0mm, No.201006-02:angle-45°/ position-1mm, No.201006-03:angle-55°/ position-0mm, No.201006-04:angle-55°/ position-1mm

In a view-point of heat input, laser-arc distance, welding speed and welding direction (leading process) were considered as main process variables in the first experiments. In the case of laser-arc distance, it is a yardstick to show the mutual interaction between laser and MIG heat source.

Heat input can be controlled by a variation of welding speed with ease. Welding direction also represents the mutual interaction between laser and MIG welding processes. The relation between bead profile, bead width in the top and bottom, and welding speed as a function of heat input was given in experiments. From the observation of bead profiles, heat transfer efficiency seems to be different according to the variation of LAD.

Fig 2. 11 was shown to be maximized in a specified LAD. That is, optimum heat transfer was occurred between LAD = 3 mm and LAD = 5 mm.

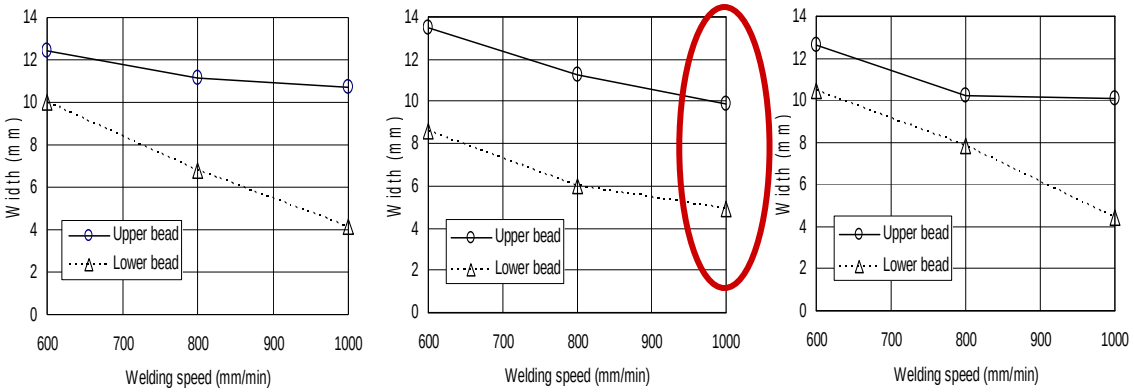

Figure 2.11 The relation between bead profile, bead width in the upper part and the lower partwelding speed for bead on plate welding by hybrid welding

2. 5. 3 Gap bridging ability

From this experiment, it is possible to select the welding condition for fillet joint and minimize the number of experiment. Specimens are prepared as shown in Fig. 2.12. From the result gap bridging ability, figure (exp. No 301006-7 & No 301006-7) have full penetration.

However, that is not optimum parameters. Also actual information and guide line on the gap bridging ability of hybrid welding process is not enough until present. Therefore, gap bridging ability of hybrid welding process has been tested with MIG and hybrid (Laser+MIG and MIG+Laser) welding processes in the varied gap conditions

In a view-point of metal structures, construction material such as aluminums plate has to be passed cutting process before the assembling process by welding. In this stage, joint line has the gap due to design and working tolerance that is to be covered by the proper welding process with productivity.

At this point, hybrid welding process has an advantage compared with the laser welding process probably. It is estimated that required heat input condition to get the full penetration will be changed according to the variation of gap condition

Therefore, careful attention for the gap and heat input control is needed to get the sound weldment in the hybrid welding process. In general, allowable gap condition is considered up to the wire diameter although intermittent full penetration is achieved in the large gap condition by sagging of molten metals.

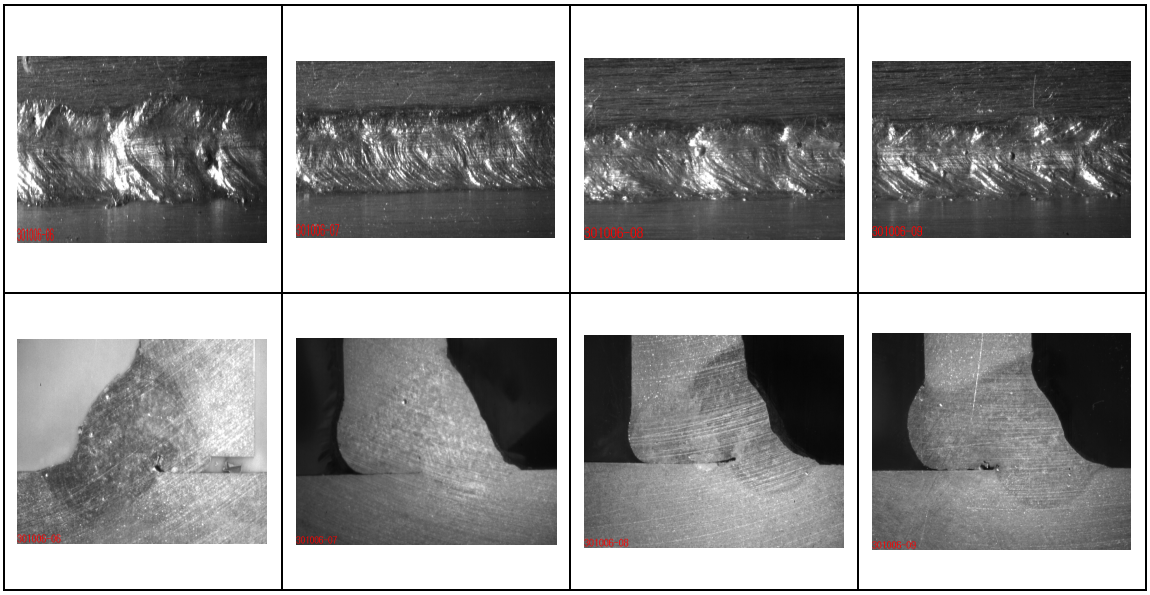

Figure 2.12 Bead shapes&Cross-section of fillet joints by Hybrid welding gap bridging ability(Laser power:3KW/194A/23.2V/Welding speed:1m/min/ combine angle:55°/Ar:20L/min/WFS:6m/min) No.201006-06:gap:0mm/focal position-1mm, No.201006-07: gap:1mm / focal position-1mm, No.201006-08: gap:1.5mm /focal position-1mm, No.201006-09: gap:2mm / position-1mm

Chapter 3 Numerical Simulation of Hybrid Welds

During the welding, the weldment is subjected to complex thermal cycles by welding heat source, so then, the residual stresses, metallurgical change and distortion are caused by thermal effect in work piece. In order to reduce these problems, it is necessary first to predict the temperature distribution that develops in the weldment.

This chapter discusses the heat distribution in laser-MIG hybrid weldment, MIG-laser hybrid weldment using the Finite Element Analysis.

In order for accurate analysis of the heat distribution in weldment, the following conditions are taken into consideration.

1) Two dimensional un-steady state heat distribution analysis is conducted using 4-node iso-parametric element.
2) The thermal coefficient of material varies with the temperature and the thermal conduction is treated as non-linear function.
3) The thermal conduction to the inside of material and the thermal transfer to the air are treated as a thermal boundary condition.
4) The material is iso-tropic media, so that is properties at each point are the same along all directions and the initial temperature is 20℃.

Fig. 3.1~3.3 shows the thermal coefficient of Al 5083 alloy, considered for welding heat distribution simulation.

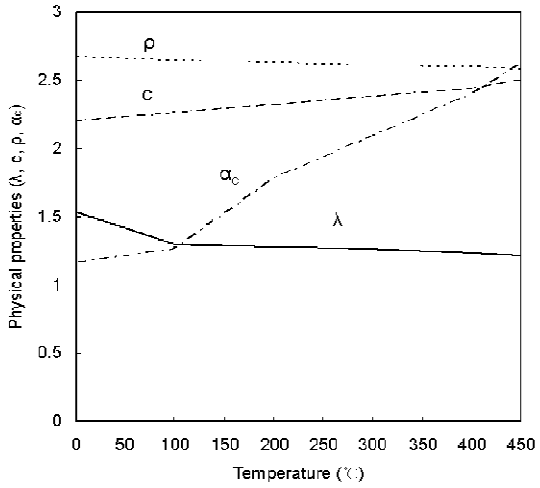

Figure. 3.1 Physical properties of Al 5083 and Al 5356 for heat conduction analysis

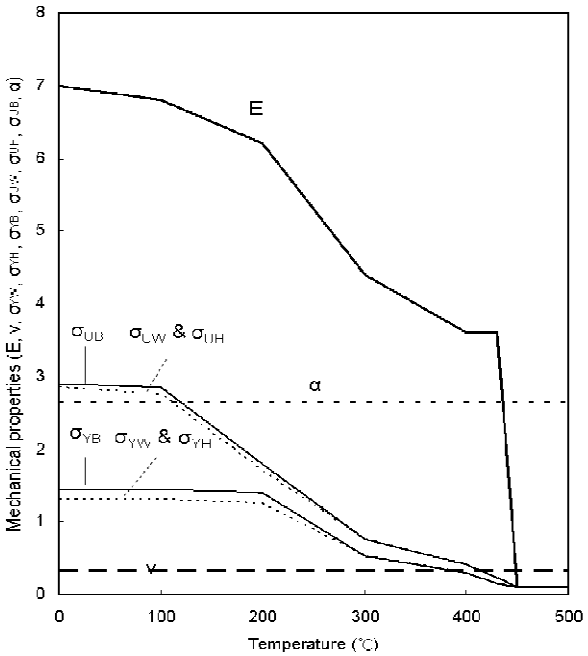

Figure. 3.2 Mechanical properties for thermal elasto-plastic analysis

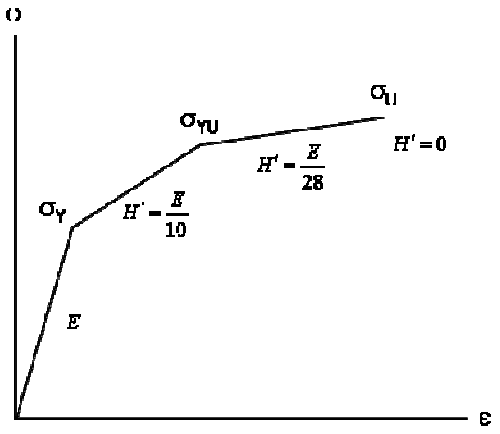

Figure. 3.3 Strain-hardening parameter for thermal elasto-plastic analysis (Al 5083)

For the analysis, the system is divided into many elements by fine mesh. The mesh model generated consist of the total Nodes = 4411 and the total elements = 4000 as shown in fig. 3.4. The temperature dependent material properties of A5083 have been used. The temperatures of all the wall elements are specified as boundary condition and temperature of the weld zone is given as heat input in (cal/mm) to the weld zone elements. The heat input in the weld zone is dissipated via conduction in to the work piece. After the analysis the temperature distribution and the thermal history of the nodes

has been determined using which residual stress distribution could be calculated. The boundary condition employed for the thermal elasto-plastic analysis is illustrated in Fig. 3.5.

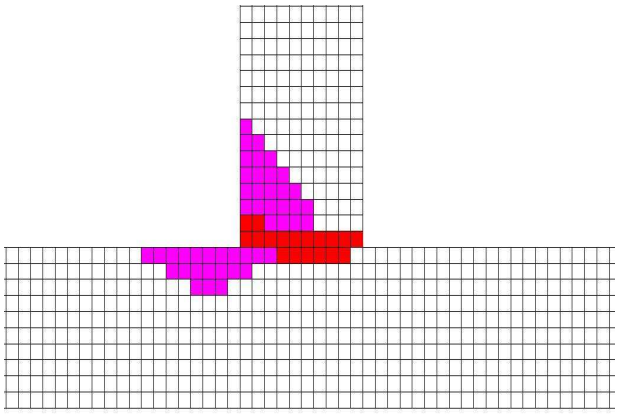

Figure. 3.4 Mesh division of weldments

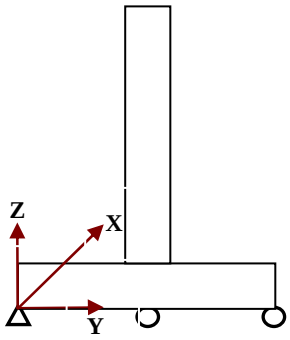

Figure. 3.5 Boundary Condition for thermal elasto-plastic analysis

From the equation (3.1) (3.2), the heat input, Q, is determined. Also each welding arc and laser efficiency is 80% and 60%. From the MIG welding process, the total transfer of heat ($H.I$) to the weldment per unit time and unit length is given by:

$$H.I = \eta_A \frac{EI}{V} \qquad (3.1)$$

where E is voltage, I is current, V is welding speed, and η_A is the heat transfer efficiency. From the laser welding process, the total transfer of heat ($H.I$) to the weldment per unit time and unit length can be given simply as follows:

$$H.I = \eta_L \frac{P}{V} \tag{3. 2}$$

where P_W is beam power of laser at workpiece, V is welding speed, and η_L is the heat transfer efficiency.

Simulation conditions for laser-MIG hybrid weldment and MIG-laser hybrid weldment are same as experimental condition.

3. 1 Thermal distribution of Hybrid welding

Fig. 3.6 shows the temperature distribution phenomenon of laser-MIG hybrid fillet weldment and MIG-laser hybrid fillet weldment. The welding heat source penetrates the welds and conducts along the flange and web of workpiece in weldment as a line heat source does. The welding condition applied for simulation is described at Chapter 2.

Laser–Arc Hybrid

Arc – Laser Hybrid

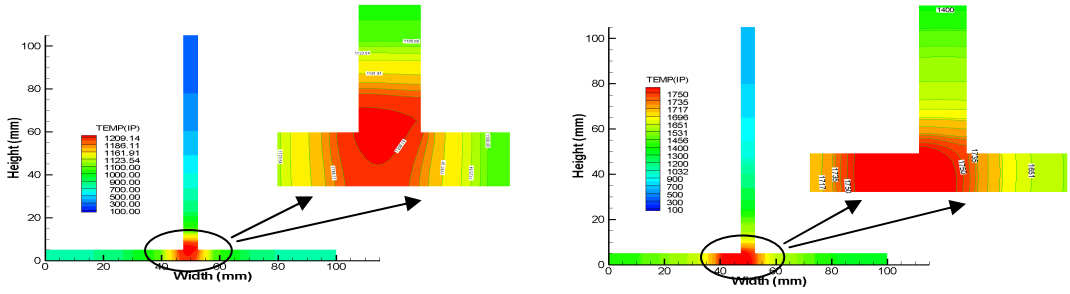

Figure. 3.6 Thermal distribution of the Laser-Arc welding, Arc-Laser welding

The welding heat transfers into flange and web of workpiece along the all direction uniformly in laser-MIG hybrid fillet weldment. And it spreads more deeply into flange and web of the workpiece. Furthermore, the welds of the laser-MIG hybrid fillet welding cools at the faster rate than does the welds of the MIG-laser hybrid fillet welding, Also the area which shows the high magnitude of hardness is formed widely in MIG-laser hybrid fillet welds.

3. 2 Thermal history of Hybrid welding

Fig. 3.7 describe the temperature increase and cooling rate in both weld metal and heat-affected-zone as a function of temperature and time.

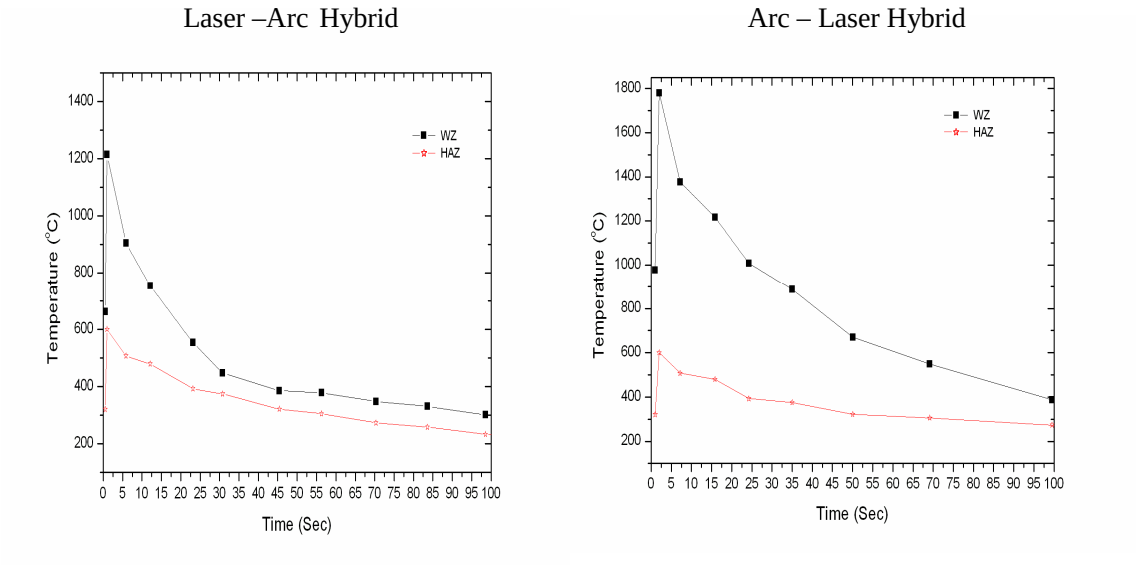

Figure. 3.7 Thermal history in Laser-Arc welding, Arc-Laser welding

From the thermal history curves in both fillet weldments, it can be assumed that the heat generated by welding heat source in laser-MIG hybrid fillet weldment dissipates at a faster rate to the area near the welds and in MIG-laser hybrid fillet weldment, the area affected by welding heat source is wider than that in laser-MIG hybrid fillet weldment, so then, the hardness is higher in laser-MIG hybrid fillet weldment and the hardness area is wider in MIG-laser hybrid fillet weldment

3. 3 Welding Residual Stress Distribution in Weldment

During the welding, the weldment is heated locally by the welding and undergoes temperature change that causes the complex strains and non-elastic strain in weld metal and the base metal near the welds. After welding, the residual stresses produced by the strain remains in weldment. This section mainly concentrates on the welding residual stresses caused by welding in MIG-laser hybrid fillet weldments and laser-MIG hybrid fillet weldments, especially, the longitudinal stresses (σ_x), acting parallel and the transverse stresses (σ_y), acting perpendicular to the direction of the weld bead.

In order to analyze the welding residual stresses in MIG-laser and laser-MIG fillet weldment using

the thermal elastic-plastic numerical simulation program, the following conditions are adopted, and the thermal histories obtained from the heat distribution analysis is used as the input data.

1. The temperature dependencies of mechanical properties (yield stress, young's modulus, thermal expansion coefficient) of Aluminum 5083 alloy are considered.
2. The solid is isotropic media.
3. The plane deformation (plane stress, plane strain) is assumed in weldment for the two-dimensional thermal elastic-plastic analysis.
4. The size and distribution of welding heat source are treated as thermal load.
5. The phase transformation effect is not considered in the present analysis.

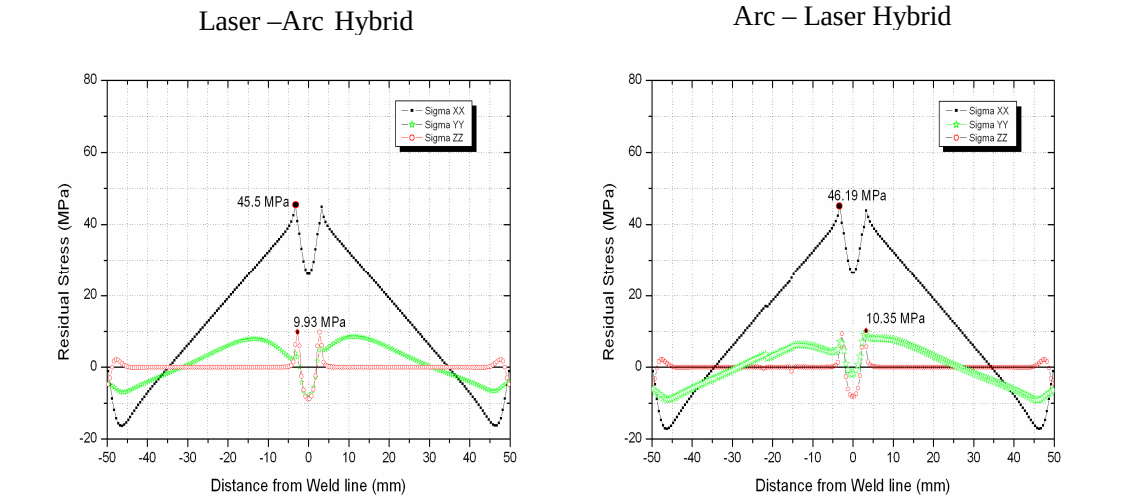

Figure. 3.8 Residual stress distribution in Laser-Arc welding, Arc-Laser welding

Fig. 3.8 shows residual stress of laser-MIG hybrid fillet weldment and MIG-laser hybrid fillet weldment. In case of hybrid fillet welding is constructed by the full-penetration welding, the residual distribution pattern is symmetrical and narrow. When comparing the characteristics of the highest residual stress in both weldments, the maximum residual stress in each hybrid fillet weldment is formed at the welding direction of welds. In case of laser-MIG fillet welding, the maximum residual stress of welding direction is 45.5MPa and in case of MIG-laser fillet welding is 46.19MPa. The high residual stress pattern at the weldment distribution in a large region around the weld line of MIG-laser fillet welding.

3.4 Heat input details

Compared with simulation, the optimization of welding process parameter, sound weld seam is achieved for gap=1 mm, focal position = 1 mm and combine angle = 55° condition with increase of welding speed up to 1000 mm/min by one(1) pass running. The optimization of welding condition was formed more deeply penetration into flange and web of the workpiece. Fig. 3.9 shows schematic diagram the optimization of welding process parameter. Also heat distribution was formed more deeply to flange and web of the workpiece.

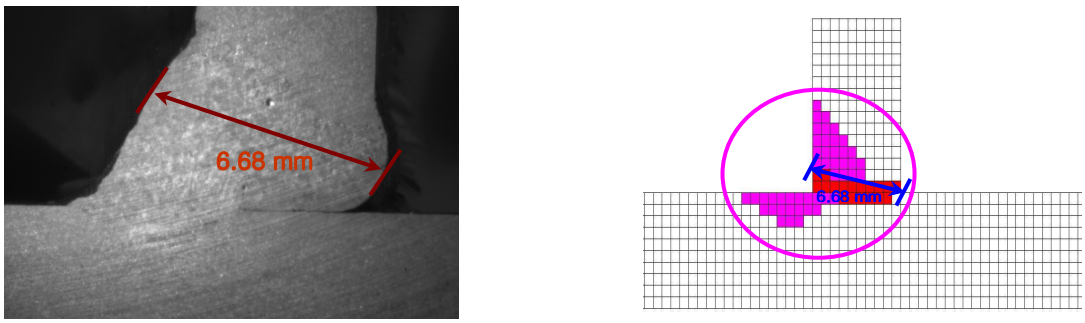

Figure. 3.9 Schematic diagram of the optimization welding condition

Fig. 3.10 shows the penetration depth variations based on the focal position gap width and angle between the welding axis and flange plate.

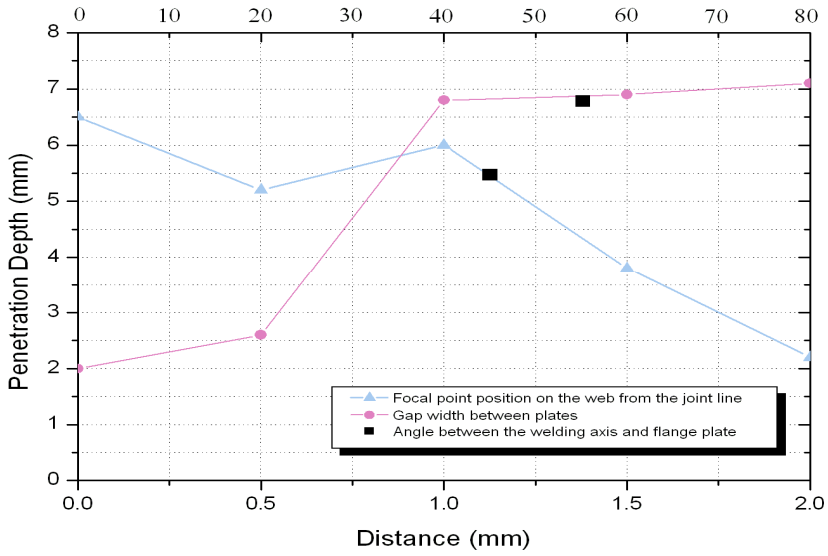

Figure. 3.10 Penetration depth variations based on the focal position gap width and angle between the welding axis and flange plate.

Chapter 4 Mechanical strength Test

4. 1 Hardness in welds

A micro hardness measurement was made on transverse sections of the weldments(201006-07). A load of 500 g and 0.5 mm between the indentations were used. Measured values of each weld are shown Fig. 4.1.

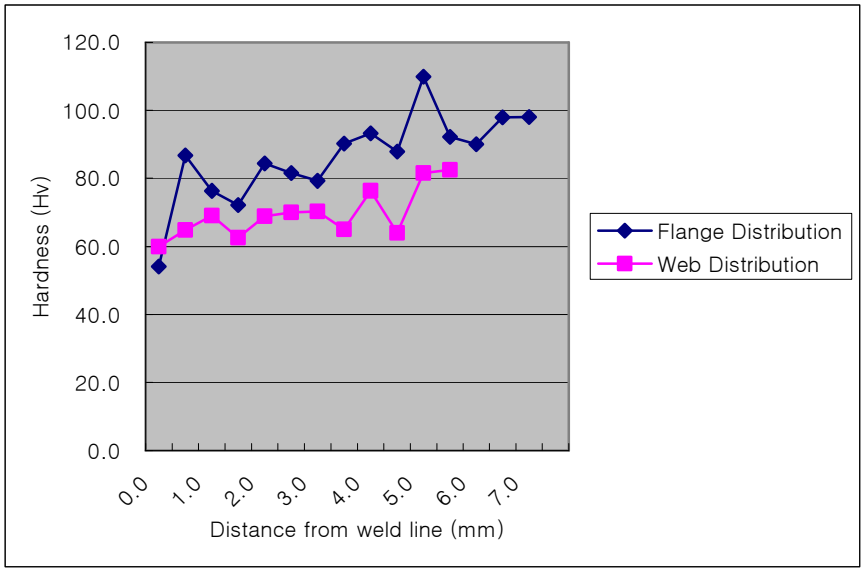

Figure. 4.1 Hardness value in Hybrid Welds(Laser+MIG)

From the test result of hardness shown in above figures, it is understand that the hardness of weld metal (WM) has the lowest value than other areas and corresponding loss of strength to the vaporization of Mg and thus a reduction in solid solution strengthening. Hardness value of the heat affected zone (HAZ) has the intermediate value between weld metal (WM) and base metal (BM) in general.

Comparing the hardness value of laser-MIG hybrid fillet welding in WM and HAZ, hardness of flange shows the high value between 50 Hv and 90 Hv. In case hardness of web, the value is formed between 60 Hv and 80 Hv. It is known that strength of metal has the relation being proportional with the hardness value. Therefore, it can be estimated that the strength of WM and HAZ are reduced in the hybrid welds compared with the strength of BM.

Chapter 5 Conclusion

Hybrid welding on fillet joints of 5 mm Al 5083 alloy is considered as follows.

1. Through the optimization of welding process parameter, sound weld seam is achieved for gap=1 mm, focal position = 1 mm and combine angle = 55° condition with increase of welding speed up to 1000 mm/min by one(1) pass running.

2. In the case of MIG welding for fillet joints, welding speed about 1000mm/min is too fast to form sufficient weld bead shape. Furthermore, web and flange were not welded completely because of incomplete fusion. However, the 600 and 700mm/min were quite good for making proper weld bead except throat size and leg length.

3. Compared with laser welding and MIG welding, penetration depth in laser-arc hybrid welding is greatly increased due to improvement of laser beam absorption. Furthermore, laser beam produces a stabilized arc in hybrid welding.

4. In MIG leading case, occurrence of contamination & spatter were increased with laser leading condition. Moreover, it seems to be humping beads because welding speed was too fast with strong arc force and incomplete fusion.

5. In hybrid fillet welding case, the welding parameters are important especially, optimization of the parameters such as focal position, combine angle etc. Gap bridging ability of the hybrid welding has been found better that arc welding and Laser welding.

6. From the result of simulation, cooling rate of WM in each process shows in the order of heat input quantity of each welding process as follows: MIG+Laser hybrid > optimum hybrid process > Laser+MIG hybrid. Calculated WM and HAZ boundary is expected well compared to experiment result. The maximum temperature value & cooling time for all the three cases has been found different and its effect on the microstructure distribution has been observed and validated experimentally.

7. Residual stress distribution in hybrid welds shows mixed shape, stress level in weld metal is increased, with GMA welds and laser welds. This tendency is also appeared in the transient stage. Stress level in weld metal is increased. In Laser+MIG hybrid welds, distribution of tensional

residual stress shows uniform value in weld metal and heat affected zone compared to other processes. Most large magnitude of residual stress in weld metal shows in hybrid welds.

8. The characteristics of hardness distribution in hybrid welds show the intermediate value between MIG and laser process. Hardness value in welds shows in the order of WM<HAZ<BM. It is known that strength of metal has the relation being proportional with the hardness value. Therefore, it can be estimated that the strength of WM and HAZ are reduced in the hybrid welds compared with the strength of BM. Effect of hardness variation in WM and HAZ and geometric bead shape are important in the strength point.

9. Thus the Hybrid fillet welding process of Al-Mg alloys was found promising for shipbuilding application using.

References

1. E. G. WEST, THE WELDING OF NON-FERROUS METALS, CHAPMAN & HALL LTD, 1951, pp.129~254.
2. Aluminum Development Council of Australia, ALUMINIUM TECHNOLOGY, Book 4: Joining Aluminum, Second Edition 1979, Cumming Enterprises Pty. Ltd. pp.57~111.
3. C M Allen, Laser welding of aluminum alloys – principles and applications, The Welding Institute REPORT, March 2004.
4. H.S. Bang and Y.P. Kim. “Fundamental Study on The Heat Input Model of Hybrid Welding for The Finite Element Analysis.” Proceedings of the 2003 Autumn Annual Meeting of Korean Welding Society, pp.36~38, 2003. (in Korean)
5. Yukio Ueda, You Chul Kim, Teruhisa Yamakita and Han Sur Bang. “Applicability of Substituting Plane-deformation Problems for Three-dimensional Thermal Elasto-plastic Problems.” Journal of Japan Welding Society. Vol. 6, No.1, pp.47~53, 1988.
6. H.S. Bang and Y.C. Kim. “Analysis on The Three-Dimensional Unstationary Heat Conduction on The Welding of Thick Plates by F.E.M.” Journal of the Korean Welding Society, Vol.9, No.2, pp.37~43, Jun 1991.
7. H.S. Bang. “Study on The Mechanical Behaviour of Welded part in thick Plate - Three-dimensional Thermal Elasto-Plastic Analysis Base on Finite Element Method.” Journal of the Korean Welding Society, Vol.10, No.4, pp.37~43, December 1992.
8. Jong-Do Kim and Akira Matsunawa. “Plasma Analysis in Laser Welding of Aluminum Alloys.” IIW doc.212-893~6 and IIW doc.Ⅳ-893-96., International Institute of Welding, Budapest, Hungary, September 1-7, 1996.
9. ASM International Handbook Committee, ASM Handbook, Volume 6 Welding, Brazing, and Soldering, pp.537~540, ASM International 1993.
10. K. Behler, J. Berkmanns, A. Ehrhardt, W. Frohn. “Laser beam welding of low weight materials and structures.” Materials & Design, Vol. 18, Nos. 4/6, pp.261~267, 1997
11. WELDING HANDBOOK, Eighth Edition, Volume 3, MATERIALS AND APPLICATION PART 1, pp.100~110, AMERICAN WELDING SOCIETY.
12. Ulrich Dilthey. “Laser Arc Hybrid Welding – an Overview.” International Institute of Welding, IIW-Doc. XII – 1710-02, pp.243-248, Copenhagen 2002.
13. Klas Nilsson, Hans Engstrom, Alexander Kaplan. “Influence of Butt- and T-joint preparation in Laser Arc Hybrid Welding.” International Institute of Welding, IIW-Doc. XII – 1732-02, pp.273-284, Copenhagen 2002.

14. John Dwight, Aluminum Design and Construction, E & FN SPON, pp.75~109, 1999
15.The Aluminum Association, Properties of Aluminum Alloys, ASM International, pp.131, pp.147, 1999.
16.C H J Gerritsen, Hybrid Nd:YAG laser MAG welding of T joints in C-Mn steels for shipbuilding applications, TWI.
17.Fronius, Digital MIG/MAG welding machine Operating Instructions/ Spare Parts list, Fronius Schweissmaschinen Vertrieb GMBH & CO KG.
18.Han-Sur Bang, Young-Pyo Kim, A Study on The Reliability Evaluation of Hybrid(CW Nd:YAG Laser+MIG) Welding of Butt Joints in Al-Mg Alloy, Proceedings of the 2005 Spring Annual Meeting of ocean Engineering and Technology, pp. 575, 2005.(in Korea)

Acknowledgements

I appreciate sincerity my supervisor professor Han-Sur Bang for having provided me an opportunity to study in my research and life. I also thank him for his valuable advice and suggestions during the course of this work and all professors at Department of Naval Architecture and Ocean Engineering, Chosun University.

I would like to thank to my colleagues, Ph.D. student Rajesh.S.R, Chong-In Oh and Jae-Sun Chu, Jun-Ki Choi, Eun-Young Jeong, Yeon-Ho Kim for their help and support, who gave me with the experiments and lab life.

Finally, would like to thanks my parents, brother, sister for being a constant source of strength and support and they always shown unbounded patience and understanding towards my studies. Special, would like to extend my appreciation to my girl friend, Eun-Mi Choi and her' s family who always gave me help and encouragement.